Journal of Advanced Research 79 (2026) 521–534

Contents lists available at ScienceDirect

Journal of Advanced Research

journal homepage: www.elsevier.com/locate/jare

# Neutrophil extracellular traps-triggered hepatocellular senescence exacerbates lipotoxicity in non-alcoholic steatohepatitis

Ming Xu [1], Hao Xu [1], Yu-Wei Ling [1], Jing-Jing Liu, Ping Song, Zhi-Qiang Fang, Zhen-Sheng Yue, Juan-Li Duan *, Fei He *, Lin Wang *

*Department of Hepatobiliary Surgery, Xijing Hospital, Fourth Military Medical University, Xi'an 710032, China*

## HIGHLIGHTS

- Neutrophil extracellular traps (NETs) accumulate in patients and mouse models with NASH.
- Elimination of NETs alleviated hepatocyte senescence and hepatic steatosis in NASH mice.
- Notch signaling regulates the formation of NASH-associated NETs and cellular senescence.
- Notch signaling mitigates steatosis by reducing inflammatory cell infiltration,Myeloid-derived Notch signaling is anticipated to serve as a promising therapeutic target for NASH.

## GRAPHICAL ABSTRACT

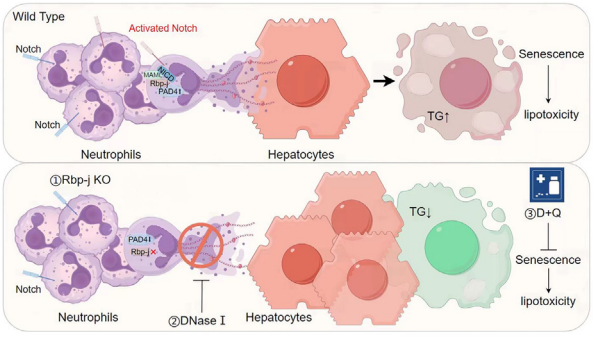


## ARTICLE INFO

*Article history:*
Received 16 December 2024
Revised 19 February 2025
Accepted 8 March 2025
Available online 9 March 2025

*Keywords:*
Neutrophil extracellular traps (NETs)
Non-alcoholic steatohepatitis (NASH)
Notch signaling
Cellular senescence
Hepatic steatosis

## ABSTRACT

*Introduction:* Neutrophils are initial responders in inflammation and contribute to non-alcoholic fatty liver disease (NAFLD) progression to steatohepatitis (NASH).

Neutrophil extracellular traps (NETs) are implicated in liver injury, yet their precise mechanisms in NASH progression remains unclear.

*Objectives:* This study investigates how NETs drive NASH progression by exacerbating hepatocyte lipotoxicity and explore the regulatory mechanism of NETs formation and its downstream effects on liver pathology.

*Methods:* Clinical samples from NASH patients and diet-induced NASH mice were analyzed for NET levels. NETs were pharmacologically inhibited, and senescent cells were selectively eliminated in mice. Myeloid-specific RBP-J knockout mice were generated to disrupt Notch signaling, with subsequent evaluation of NET formation, senescence markers, steatosis, fibrosis, and inflammation.

*Results:* NETs were elevated in NASH patients and mice, correlating with hepatocyte senescence and lipotoxicity. Pharmacological NET disruption reduced hepatocyte senescence, accompanied by attenuated steatosis and fibrosis. Senescent cell clearance replicated these improvements, confirming liver senescence emerges is a vital step for NETs to promote the progression of NASH. Myeloid-specific Notch signaling ablation suppressed NET generation, concurrently decreasing lipid deposition and liver inflammation.

* Corresponding authors.
*E-mail addresses:* duan_juan_li@126.com (J.-L. Duan), hefei_hefei@163.com (F. He), fierywang@163.com (L. Wang).
[1] Equal contribution

https://doi.org/10.1016/j.jare.2025.03.015

*Conclusion:* Our findings elucidate a novel mechanism by which neutrophil-derived Notch driven NETs exacerbate NASH by promoting cell senescence, thereby contributing to hepatic steatosis and fibrosis. This insight may provide potential intervention strategies and therapeutic targets for NASH treatment.


## Introduction

Non-alcoholic fatty liver disease (NAFLD) afflicts more than a third of the world's population and has become the most common chronic liver disease worldwide [1–3]. With the confluence of obesity, diabetes and other metabolic related factors, its incidence rate continues to escalate [4]. NASH is a critical juncture in the evolution of the NAFLD disease spectrum. If a patient is diagnosed with NASH, their risk of developing end-stage liver diseases such as cirrhosis and liver cancer increase significantly [5]. Although liver immune disorders and lipotoxicity are considered the primary pathogenic factors, due to the elusive etiology, impedes the development of curative and effective treatment strategy for NASH [6,7].

Inflammatory infiltration characterizes the pathological landscape of NAFLD, and neutrophils, as the first responders of inflammation notably, play an indispensable role in the evolution from simple hepatic steatosis to NASH [8–10]. Traditionally, neutrophils have been recognized primarily for their roles as antigen-presenting cells and which include stimulating macrophage recruitment. However, recent studies have expanded this view by demonstrating that neutrophils also advance NAFLD progression through the production of NETs [11]. NETs, intricate DNA network structures released by neutrophils in response to various damage stimuli, are attached with proteins such as citrullinated histone H3 (CitH3) and myeloperoxidase (MPO) [12]. Increasing evidence links that NETs are closely related to various acute and chronic liver injuries, where their accumulation initiates a series of inflammatory responses [13–17]. Therefore, delineating the origins and impacts of NETs in NAFLD may offer innovative strategies for managing this disorder.

Cellular senescence denotes an irreversible state of cell cycle arrest induced by a variety of endogenous or exogenous factors, including telomere shortening, DNA damage, epigenetic disorders, and mitochondrial dysfunction [18]. Senescent cells not only undergo morphological changes but also alter the secretion of inflammatory cytokines [19]. Recognized cellular senescence biomarkers in scientific literature include SA-β-Gal, p16, p53 and p21 [18,20,21]. Senescent cells not only contribute to bodily senescence but also foster various diseases and metabolic disorders through the senescence of different cell types [22]. Cellular senescence also precipitates adipose degeneration, a metabolic disorder [23]. Research has revealed that liver cells in NAFLD patients manifest senescent characteristics, notably severe DNA damage and cell cycle arrest [24]. Despite these findings, the precise mechanisms at play warrant further investigation [25].

The Notch signaling pathway, a short-range signal transduction mechanism mediated by transmembrane ligand-receptor interactions, plays a pivotal role in development, tissue and organ homeostasis maintenance, and disease onset and progression [26]. Studies have identified Notch and its downstream molecules as key regulators of liver physiological metabolism, liver fibrosis, repair and regeneration, and liver cancer occurrence [27,28]. Notably, the roles of liver cells and non-parenchymal cell-derived Notch, notably from liver sinusoidal endothelial cells (LSECs), in NAFLD have been investigated and reported [29]. However, research on the impact of immune cell-derived Notch signaling, such as neutrophils, on liver diseases including NAFLD remains scarce. Examining this area is essential for a comprehensive understanding of the intricate relationship between Notch signaling, liver metabolism, and associated pathologies.

In this study, we performed rigorous in vivo and in vitro experiments using clinical samples and mouse models to examine the role of neutrophils in driving liver cell senescence by regulating NETs formation, thereby promoting lipotoxicity and disease progression. Additionally, we elucidated the role of neutrophil-derived Notch signaling in the onset and development of NASH. Our findings may provide novel insights and potential therapeutic targets for NASH treatment.

## Materials and methods

### Mice

C57BL/6 wild-type mice were purchased from Gempharmatech Co., Ltd., *Lyz2-Cre; RBPJ$^{flox}$* mice were donated by Prof. Han Hua of the Fourth Military Medical University. *Lyz2-Cre; RBPJ$^{flox/flox}$* (RBPJ-KO) littermate *Lyz2-Cre; RBPJ$^{flox/+}$* or wild C57BL/6 mice were used as controls. Experimental NAFLD mouse model was induced by feeding either the choline-deficient L-amino acid diet (CDAA) for 10 weeks or the methionine and choline-deficient diet (MCD) for 6 weeks to 7–8 week-old male mice. In order to eliminate NETs in NASH mice, DNase I (Roche, China) was diluted with PBS and formulated into a concentration of 100 μg/mL. According to the body weight of the mice, DNase I was injected intraperitoneally at a dose of 2.5 μg/g, 3 times a week, at the beginning of the 4th week of modeling in MCD mice, and samples were sacrificed until the 6th week. The control group used PBS. In order to eliminate senescent cells in NASH mice, the drug was dissolved with 4 % DMSO, 30 % PEG300, 2.5 % Tween 80 and 61 % dd$H_2O$, and Dasatinib&Quercetin (DQ) gavage was administered to MCD mice at doses of dasatinib 5 mg/kg and quercetin 50 mg/kg, 3 times a week, starting at the 4th week of modeling until the sixth week. The control group was treated with equal proportion solvent.

All laboratory animals are housed in SPF-rated animal houses, and all animal experiments are conducted in accordance with the guidelines of the the Fourth Military Medical University Animal Laboratory Management Board.

### Serum and liver tissue samples of patients

Serum and liver tissue samples (paraffin-embedded liver tissue) from NASH patients were obtained from the Department of Hepatobiliary Surgery, Xijing Hospital, the Fourth Military Medical University. The patients with NASH were clinically and pathologically diagnosed, while the control group was non-diabetic, non-alcoholic, or non-viral hepatitis patients. Basic patient information is listed in Table S1. All participants have signed informed consent. Clinical samples involving humans are approved by the Ethics Committee of Xijing Hospital, the Fourth Military Military Medical University.

### Histology assay

Liver tissue was fixed with 4 % paraformaldehyde. Paraffin and frozen sections were prepared according to the previously

described protocol, and Hematoxylin and Eosin (H&E) staining, Sirius Red staining, immunofluorescence (IF) staining, and immunohistochemical (IHC) staining were performed (Antibodies were used in Table S2). The saturated Oil Red O solution was purchased from Servicebio (G1015-100 mL, Wuhan, China), and the SA-β-gal staining kit was purchased from Beyotime (C0602, Shanghai, China). Fresh liver tissue was stained according to the product instructions.

### *Biochemistry and Enzyme-linked immunosorbent assay (ELISA)*

Serum levels of alanine aminotransferase (ALT), aspartate aminotransferase (AST), total triglycerides (TGs) were determined using commercially available kits (Rayto, Shenzhen, China) and measured using an automated biochemical analyzer (Chemray 800, Rayto, China). TC and TG levels in liver tissue were measured using commercially available kits (Applygen, Beijing, China). The levels of MPO in serum were measured using kits from Liankebio (Zhejiang, China) following the manufacturer's protocols.

### *Neutrophil isolation and NETs extraction*

Neutrophils from human peripheral blood were isolated by gradient centrifugation. Peripheral venous blood was collected from healthy subjects using anticoagulant tubes, and 15 mL centrifuge tube is added successively from bottom to top: 5 mL 1119 lymphocyte isolation solution (Sigam, USA) → 2 mL 1077 lymphocyte isolation solution (Sigam, USA) → 5 mL-7 mL peripheral blood whole blood. Then 4 ℃, 750 g, slowly rise slowly fall, centrifuge for 30 min. After centrifugation, the plasma layer, PBMCs layer and liquid separation layer were discarded, and neutrophils layer were collected, and add with about 5 mL red blood cell lysis buffer (Solarbio, Beijing, China), which was cracked at 4℃ for 15 min and then again. Neutrophil precipitation was obtained by centrifugation at 450 g for 10 min (the erythrocyte Lysing step was repeated until no red blood cells were found in the precipitation). Finally, about 5 mL PBS was added to wash the cell precipitation, and after blowing evenly, the supernatant was discarded after being centrifuged at 4℃ and 450 g for 5 min. Leukocyte precipitations were suspended in a complete medium containing 1640 RPMI. For mouse bone marrow neutrophils, bone marrow cell suspensions were collected from the femur and tibia of mice, and the neutrophils were isolated by gradient centrifugation as in peripheral blood.

Mouse bone marrow neutrophils were isolated from the femur and tibia of mice. After the bone marrow suspension was collected, gradient centrifugation was performed using 1119 and 1077, and the remaining steps were the same as above.

The suspended neutrophils were planted in a 10 $cm^2$ petri dish, added with 90 nM PMA, placed in an incubator at 37 ℃ and 5 % $CO_2$ for 4 h, then the supernatant was discarded, the residual medium was gently rinsed with sterile PBS, and the flocculent attachment at the bottom of the petri dish was rinsed with clean sterile PBS and collected into a 15 mL centrifuge tube. After full blowing, the supernatant containing NETs was obtained by centrifugation at 450 g at 4 ℃ for 10 min and frozen at −80 ℃ for storage. NETs were quantified according to instructions with Quant-iT™ PicoGreen™ dsDNA Reagent and Kit from Thermo Fisher Scientific (MA, USA) prior to use.

### *Primary hepatocyte isolation*

Primary hepatocyte were isolated from liver tissues as previously described [30].

### *Cell culture*

Alpha mouse liver 12 (AML12) cells were cultured in Special medium for AML12 cells (Procell, Wuhan, China), added with the fresh medium containing different concentrations NETs for 48–72 h, and primary hepatocyte were cultured in DMEM without FBS, added with the fresh medium containing 300 μM $H_2O_2$ or NETs for 24 h. Then the treated AML12 or primary hepatocyte cells were stained with Oil Red O (Servicebio, Wuhan, China) and SA-β-gal (Beyotime, Shanghai, China). Triglyceride content in the treated AML12 or primary hepatocyte cells was measured using a detection kit (Applygen, Beijing, China) following the manufacturer's protocols.

PMN were treated with γ-secretase inhibitor N-[N-(3,5-Difluor ophenacetyl)-L-alanyl]-S-phenylglycine t-butyl Ester (DAPT, 5 μM, Selleck, USA) or DMSO for 24 h, changed and cultured with the fresh medium containing PMA for 2 h, and the conditioned medium (CM) were harvested, then determining NETs concentration according to instructions with Quant-iT™ PicoGreen™ dsDNA Reagent and Kit.

### *Western blot*

Total protein of liver tissues was extracted using RIPA lysis buffer (Beyotime, Shanghai, China) containing phenylmethylsulfonyl fluoride (PSMF, 10 mM), and the protein concentration was quantified using the BCA Protein Assay Kit (Beyotime, Shanghai, China) following the manufacturer's instructions. The samples were analyzed by SDS-PAGE, transferred to PVDF membranes (Millipore, Billerica, MA, USA), blocked with 5 % skimmed milk powder, and incubated with primary antibodies targeting MPO, CitH3, P16, P21 and P53 overnight at 4 ℃, and then with HRP-conjugated goat anti-mouse or anti-rabbit IgG secondary antibodies. The information of the antibodies used is listed in Table S2.

### *RNA extraction and Real- time quantitative PCR assay (RT-qPCR)*

Extract RNA from cells and tissues by TRIzol reagent (Invitrogen,USA) and reverse transcribed the mRNA into cDNA using Evo M-MLV RT Premix (Accurate Biology, Changsha, China). Quantitative PCR (qPCR) was performed using SYBR Green PCR Master Mix (Accurate Biology) according to the manufacturer's protocol. Relative gene expression levels were normalized to those of β-actin or Gapdh. All primers were purchased from Tsingke Biotechnology Co. Ltd. (Beijing, China). The sequences of the primers used in the current article are listed in Table S3 and Table S4.

### *RNA sequencing and bioinformatics analysis*

Establish a CDAA model with *Lyz2-Cre; RBP-J$^{flox/flox}$* (RBPJ-KO) and *Lyz2-Cre; RBPJ$^{flox/-}$* (CT) mice, and obtain liver tissue for RNA-sequencing (RNA-seq). Bioinformatics analyses, including Gene Ontology (GO) enrichment analysis and Kyoto Encyclopedia of Genes and Genomes (KEGG) enrichment analysis, were performed using OmicShare Tools (*https://www.omicshare.com/tools*). Gene set enrichment analysis (GSEA) was conducted using gene sets from the Molecular Signature Database (MSigDB) 4.0.

### *Statistical analysis*

The morphological results were quantitatively analyzed by Image Pro Plus 6.0 software, the gray values of WB luminescent bands were analyzed by Image J software, and the statistical data were analyzed and mapped by Graph Pad Prism 8 software. Unpaired T-test was used to compare the differences between the two groups of continuous variables, differences among multi-

ple groups were compared using one-way ANOVA, and the data were expressed as means ± SD, and the difference of $P < 0.05$ was statistically significant.

## Results

### *NETs accumulate both in NASH patients and mice*

To ascertain the clinical relevance, we initially collected blood and liver tissue samples from both patients with NASH and healthy subjects to measure the serum levels of NETs-related free dsDNA. We detected elevated levels of NETs in the peripheral blood of NASH patients (Fig. 1A). Subsequently, we confirmed this observation in a diet-induced NASH mouse model; serum tests indicated a marked increase in NETs-related free dsDNA levels in NASH mice (Fig. 1B). To further investigate molecules associated with NETs, we analyzed the protein expression of MPO and CitH3 in liver tissues from NASH and control mice (Fig. 1C, D), and observed that these proteins were similarly elevated in the liver tissues of NASH mice. Additionally, we conducted MPO IHC staining (Fig. 1E) and CitH3 IF staining (Fig. 1G) on liver tissue sections of NASH patients, and the positive area measurements (Fig. 1F, H) indicated an increase in NETs formation in the liver tissues of NASH patients. These findings demonstrate that NETs are accumulated in both NASH patients and mice.

### *NETs induce senescence and lipotoxicity in hepatocytes*

To investigate the specific association between NETs and hepatocyte senescence as well as lipid deposition, we collected peripheral blood from healthy subjects, from which we isolated neutrophils. We stimulated the neutrophils with PMA to generate NETs in vitro, which we then quantified and introduced into the culture medium of the AML-12 hepatocyte line at concentration gradients of 100 ng/mL, 200 ng/mL, and 500 ng/mL. Following a 48–72 h treatment period, the mRNA expression levels of senescent-related molecules P16, P21, P53, and GATA4 were measured using qPCR (Fig. 2A). We observed an increased expression of these senescent-related molecules in AML-12 cells post NETs treatment. Meanwhile, given that SA-β-gal is currently recognized as a marker of cellular senescence, we detected its expression in AML-12 and primary hepatocytes via staining (Fig. S1, Fig. 2B). Subsequent statistical analysis revealed a higher proportion of SA-β-gal$^+$ cells in the NETs treatment group compared to the control group (Fig. S1, Fig. 2C), suggesting that NETs can stimulate hepatocyte senescence. Additionally, we observed lipid deposition in

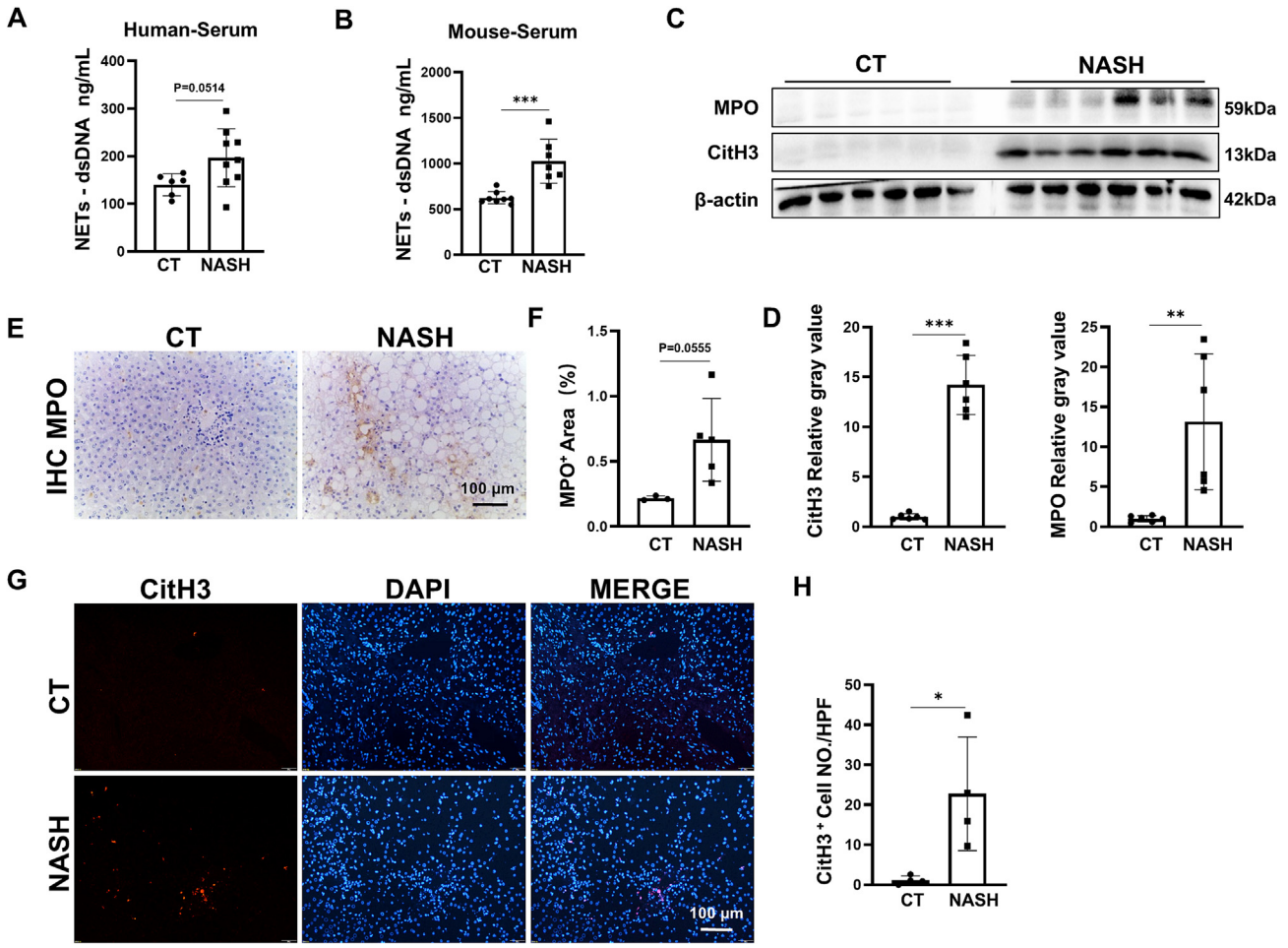


**Fig. 1.** NETs are accumulated in NASH patients and mice. (A) Serum NETs-dsDNA concentrations in NASH patients and healthy subjects ($n$ = 6 to 9). (B) Serum NETs-dsDNA concentrations in NASH and control mice ($n$ = 4 to 5). (C) Protein expression and (D) statistics of MPO and CitH3 in liver tissues of NASH mice and control mice ($n$ = 6). (E) IHC staining of MPO in liver tissues of NASH patients and healthy subjects and (F) positive area statistics ($n$ = 3 to 5). Scale bar: 100 μm. (G) IF staining of CitH3 in liver tissues of NASH patients and healthy subjects and (H) positive cell number statistics ($n$ = 4). Scale bar: 100 μm. Bars represent means ± SD; $^*P < 0.05$, $^{**}P < 0.01$, $^{***}P < 0.001$.

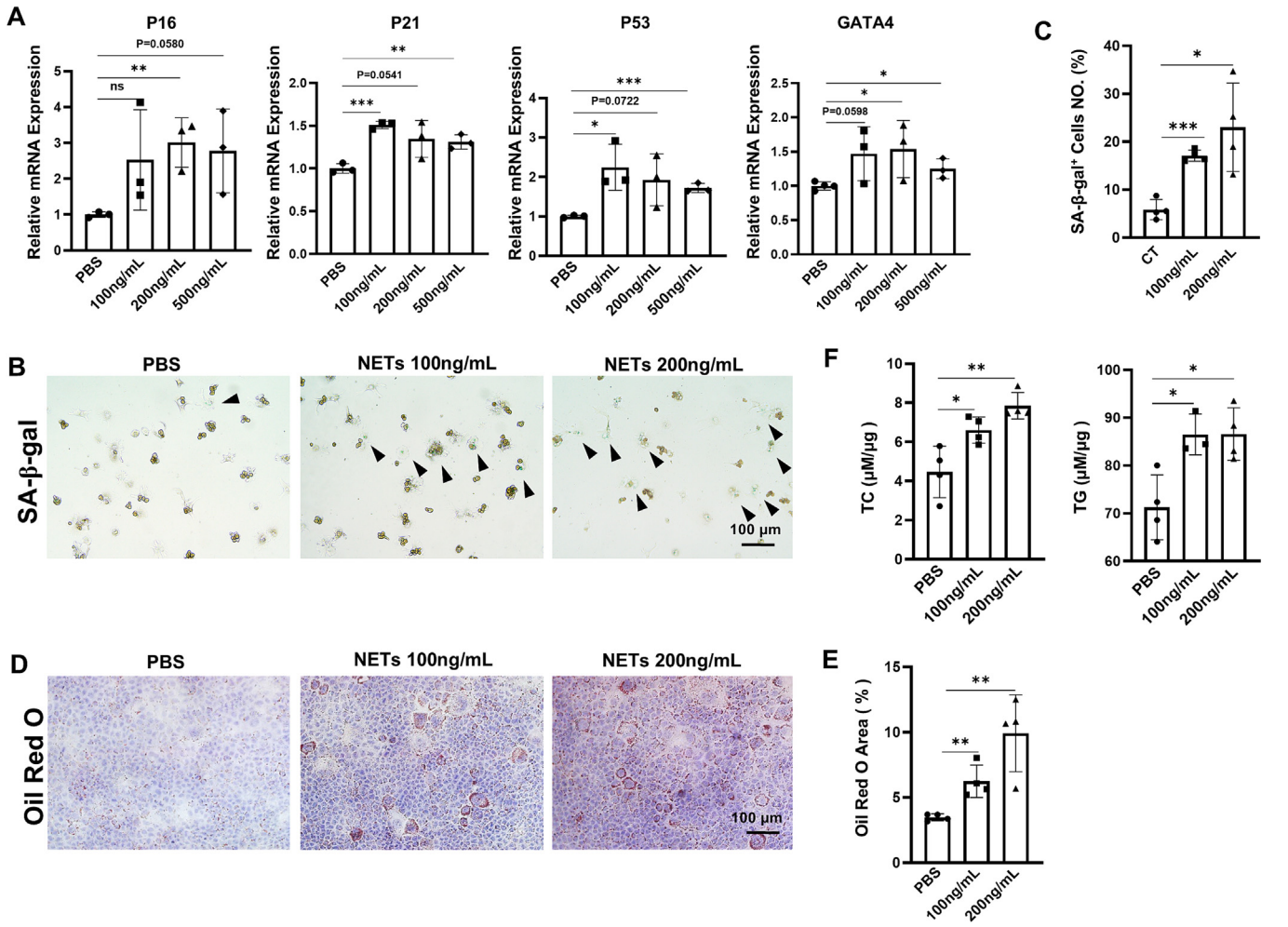


**Fig. 2.** NETs triggered hepatocyte senescence and lipotoxicity. (A) Relative mRNA expression levels of P16, P21, P53 and GATA4 in AML-12 cells after concentration gradient of control and NETs treatment were determined using qPCR; β-actin served as an internal control ($n = 3$). (B) SA-β-gal staining of primary hepatocytes cells after PBS and NETs treatment, and (C) SA-β-gal$^+$ cells were quantitatively compared ($n = 4$). Scale bar: 100 μm. (D) Oil Red O staining of AML-12 cells after PBS and NETs treatment, and (E) positive areas of staining were quantitatively compared ($n = 4$). Scale bar: 100 μm. (F) Hepatic TC and TG levels were evaluated in AML-12 cells after PBS and NETs treatment ($n = 4$). Bars represent means ± SD; $^*P < 0.05$, $^{**}P < 0.01$, $^{***}P < 0.001$, ns, not significant.

AML-12 cells following NETs treatment. Oil Red O staining indicated a significant accumulation of lipid droplets in hepatocytes of the NETs treatment group (Fig. 2D). Statistical analysis suggested that NETs exacerbate lipid deposition in hepatocytes (Fig. 2E). Further, we measured the TC and TG content in AML-12 cells post NETs treatment (Fig. 2F) and noted a significant elevation in hepatocyte TC and TG content in the NETs treatment group. Collectively, these results suggest that NETs promote hepatocyte steatosis in vitro, concurrent with hepatocyte senescence.

*Abrogating NETs alleviates cellular senescence and hepatic steatosis in NASH mice*

To further elucidate the impact of NETs on liver function and lipid metabolism during NASH progression, we performed an in vivo intervention experiment employing a diet-induced NASH mouse model. DNaseI was intraperitoneally administered to the mice from the fourth week of the MCD modeling period and continued until the sixth week to eliminate NETs. Serum analysis, IHC staining and Western blot of MPO revealed a significant increase in MPO content of NASH mice, which was reduced after NETs clearance, IF staining of CitH3 also demonstrated similar changes, all of which indicate successful modeling (Fig. S2A-E). Additionally, liver tissue AST and ALT results further emphasized significant hepatic dysfunction in NASH mice, which was partially ameliorated following NETs clearance (Fig. S2F). This infers that NETs accumulation exacerbates hepatic injury in NASH, and NETs clearance partially mitigates such injury. Moreover, we examined the effect of NETs clearance on liver senescence in NASH mice. Staining of murine hepatic tissue sections revealed a significant elevation in SA-β-gal content in the NASH group, which was suppressed following DNaseI treatment (Fig. 3A, B). To bolster the reliability of our conclusion, we also examined the expression of representative molecules in the senescence-associated secretory phenotype (SASP). IHC staining for P21 showed increased expression in the liver tissue of NASH mice compared to control mice, which was downregulated after DNaseI treatment (Fig. 3C, D). In addition, Western blot analysis of hepatic tissue from mice subjected to different interventions unveiled increased protein expression levels of P21 and P53 in the NASH group, which were suppressed following DNaseI treatment (Fig. 3E, F). Similarly, we used qPCR to detect changes in the expression of some representative molecules in the SASP. We found that DNaseI injection had no significant effect on the expression of SASP-related molecules in control mice, but inhibited their expression in the NASH mice treated with DNaseI compared to those treated with PBS (Fig. 3G).

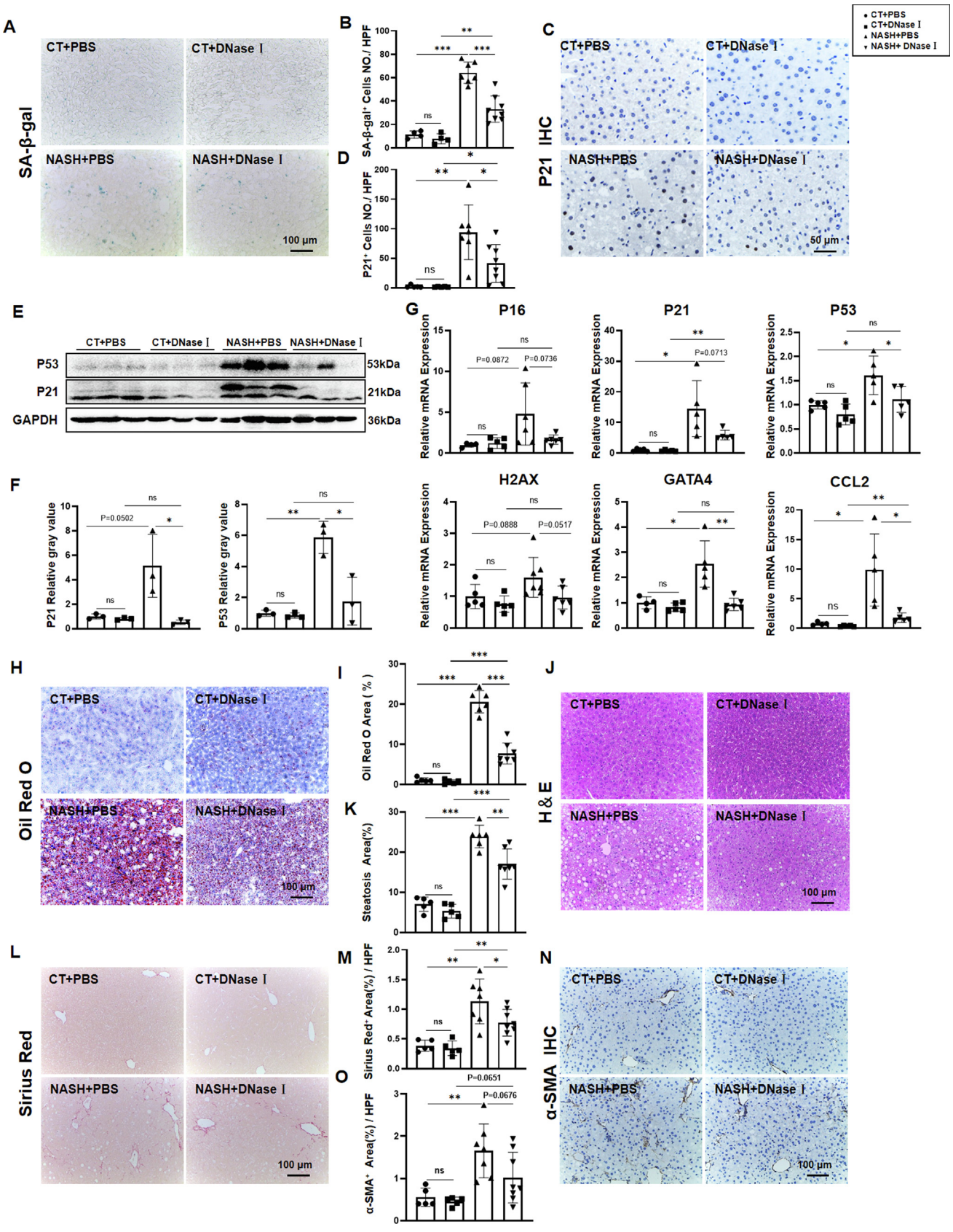
A
SA-β-gal
CT+PBS
CT+DNase I
NASH+PBS
NASH+DNase I
100 μm
B
SA-β-gal⁺ Cells NO./ HPF
C
IHC
P21
50 μm
D
P21⁺ Cells NO./ HPF
E
P53
P21
GAPDH
53kDa
21kDa
36kDa
F
P21 Relative gray value
P53 Relative gray value
G
P16
P21
P53
H2AX
GATA4
CCL2
Relative mRNA Expression
H
Oil Red O
I
Oil Red O Area ( % )
J
H & E
K
Steatosis Area(%)
L
Sirius Red
M
Sirius Red⁺ Area(%) / HPF
N
α-SMA IHC
O
α-SMA⁺ Area(%) / HPF

Therefore, we believe that NETs clearance alleviate liver cell senescence in NASH mice.

Conversely, to observe the impact of NETs clearance on hepatic steatosis in NASH mice, we conducted Oil Red O and H&E staining. Oil Red O staining (Fig. 3H) showed a significant increase in liver lipid droplets in NASH mice compared to control mice, but after DNaseI treatment, we found a significant decrease in both the number and size of liver lipid droplets in NASH mice. Statistical analysis revealed a significant decrease in the positive area of Oil Red O staining (Fig. 3I). H&E staining (Fig. 3J) showed that the number and diameter of liver fat vacuoles were also reduced after DNaseI treatment in NASH mice. Statistical analysis revealed a significant reduction in the fat vacuole area after treatment (Fig. 3K), indicating that NETs clearance partially alleviate lipid deposition in NASH. Furthermore, we performed Sirius Red staining (Fig. 3L, M), α-SMA staining (Fig. 3N, O) to evaluate the degree of hepatic fibrosis. The results suggested that hepatic fibrotic scars in NASH mice increased post DNaseI treatment, followed by a subsequent decrease upon continued treatment. Taken together, these results suggest that NETs clearance ameliorates hepatic injury, hepatocyte senescence, liver fibrosis, and steatosis in NASH mice. In addition, we also observed the number and activation status of neutrophils, macrophages and T lymphocytes, and the results showed that the number of neutrophils and macrophages were significantly reduced after DNaseI treatment, but the number of T cells did not change significantly, and no significant changes were observed in the activation status of macrophages and T cells (Fig. S4).

*Elimination of senescent cells decelerates senescence-induced hepatic steatosis*

To clarify the relationship between cellular senescence and hepatic steatosis, we initially employed an in vitro model of primary hepatocyte senescence induced by $H_2O_2$. We harvested primary hepatocytes from wild-type mice livers, facilitated their adherence overnight, and subsequently cultured them in serum-free DMEM containing 300 μM $H_2O_2$ for 24 h. We performed qPCR to ascertain the mRNA expression levels of key SASP molecules P16, P21, and P53. The results demonstrated enhanced expression of senescence-related molecules in the $H_2O_2$-induced group (Fig. 4A). Concurrently, SA-β-gal staining uncovered a significant increase in β-galactosidase activity in hepatocytes of the $H_2O_2$-induced group (Fig. 4B), suggesting the effective establishment of an in vitro model of primary hepatocyte senescence induced by $H_2O_2$. To ascertain whether cellular senescence affects lipid metabolism in hepatocytes, we conducted Oil Red O staining on $H_2O_2$-induced senescent hepatocytes. The results indicated augmented lipid deposition in hepatocytes of the $H_2O_2$-treated group (Fig. 4C), and elevated expressions of TC and TG in primary hepatocytes (Fig. 4D). Thus, we initially inferred concluded that cellular senescence exacerbate lipid deposition in hepatocytes.

Subsequently, we developed an MCD diet-induced mouse model of NASH for in vivo verification. Specifically, mice were administrated DQ via oral gavage from the fourth week of modeling, thrice weekly, until their sacrifice at the sixth week. The objective of the DQ treatment was to eradicate senescent cells during NASH progression, with the control group receiving an equivalent volume of drug solvent. Following DQ treatment, we initially evaluated the expression of SA-β-gal and SASP-related molecules in mouse liver tissue to confirm successful modeling. SA-β-gal staining results demonstrated a significant decrease in β-galactosidase-positive cells in the liver tissue of DQ-treated mice (Fig. 4E, F). Western blot analysis disclosed downregulated expressions of P16 and P21 in the liver tissue of DQ-treated mice (Fig. 4G), suggesting the successful formulation of a model for eliminating senescent cells in NASH mouse livers.

To examine the impact of eliminating senescent cells on liver lipid deposition, we conducted H&E staining on mouse liver tissue sections. The results indicated a reduction in both size and number of lipid vacuoles in the livers of NASH mice treated with DQ (Fig. 4H). Statistical analysis of the lipid vacuole area disclosed a significant decrease in the DQ-treated group. To validate these findings, we implemented Oil Red O staining and discovered a reduction in liver lipid droplets in the DQ-treated group (Fig. 4I). Additionally, we noted a decrease in the liver to body weight ratio in the DQ-treated group (Fig. 4J) and a reduction in serum TG levels (Fig. 4K), suggesting that DQ treatment partially restored lipid metabolism in NASH mice. The assessment of liver ALT and AST levels indicated a significant improvement in liver injury in the DQ-treated group (Fig. 4L). Concurrently, we employed α-SMA staining (Fig. 4M) and Sirius Red staining (Fig. 4N) to examine liver tissue, respectively. We discerned that NASH mice treated with DQ exhibited a reduction in fibrous scars and a decline in the degree of liver fibrosis. Collectively, these results propose that senescent cells contribute to liver lipid deposition and worsen liver lipotoxicity during NASH progression. The elimination of senescent cells results in improved lipid metabolism and lessened liver injury. In this model, we also observed the number and activation status of neutrophils, macrophages and T lymphocytes. The results showed that the number of neutrophils and macrophages significantly decreased after DQ treatment, and the activation of M1 type macrophages also decreased, but the number and activation status of T cells did not change significantly (Fig. S5).

*Blocking Notch signaling effectively reduces the formation of NASH-associated NETs*

Preliminary studies, inclusive of our initial work, have demonstrated the pivotal role of the Notch signaling pathway in NASH. To scrutinize the alterations in neutrophil-derived Notch signaling during this pathological process, we employed IHC staining of HES1 and LY6G on liver tissue sections from diet-induced NASH

**Fig. 3.** Abrogating NETs alleviated cellular senescence and hepatic steatosis in NASH mice. (A) SA-β-gal staining of in liver tissue, and (B) positive cells were quantitatively compared. Scale bar: 100 μm. (C) IHC staining of P21 in liver tissue, and (D) positive cells were quantitatively compared. Scale bar: 50 μm. (E) Western blot analysis of P21 and P53 protein expression in liver tissue of NASH and control mice intraperitoneally administered PBS or DNase I, and (F) the gray ratio of P21, P53 and GAPDH was quantitatively compared ($n$ = 3). (G) Relative mRNA expression levels of P16, P21, P53, H2AX, GATA4 and CCL2 in liver tissue of NASH and control mice intraperitoneally administered PBS or DNase I were determined using qPCR; β-actin served as an internal control ($n$ = 5 to 7). (H) Oil Red O staining of liver tissue of NASH and control mice intraperitoneally administered PBS or DNase I, and (I) positive area were quantitatively compared ($n$ = 5 to 7). Scale bar: 100 μm. (J) H&E staining of liver tissue of NASH and control mice intraperitoneally administered PBS or DNase I, and (K) steatosis area were quantitatively compared ($n$ = 5 to 7). Scale bar: 100 μm. (L) Sirius Red staining of liver tissue of NASH and control mice intraperitoneally administered PBS or DNase I, and (M) positive area were quantitatively compared ($n$ = 5 to 8). Scale bar: 100 μm. (N) α-SMA staining of liver tissue of NASH and control mice intraperitoneally administered PBS or DNase I, and (O) positive area were quantitatively compared ($n$ = 5 to 8). Scale bar: 100 μm. Bars represent means ± SD; $^{*}P < 0.05$, $^{**}P < 0.01$, $^{***}P < 0.001$, ns, not significant.

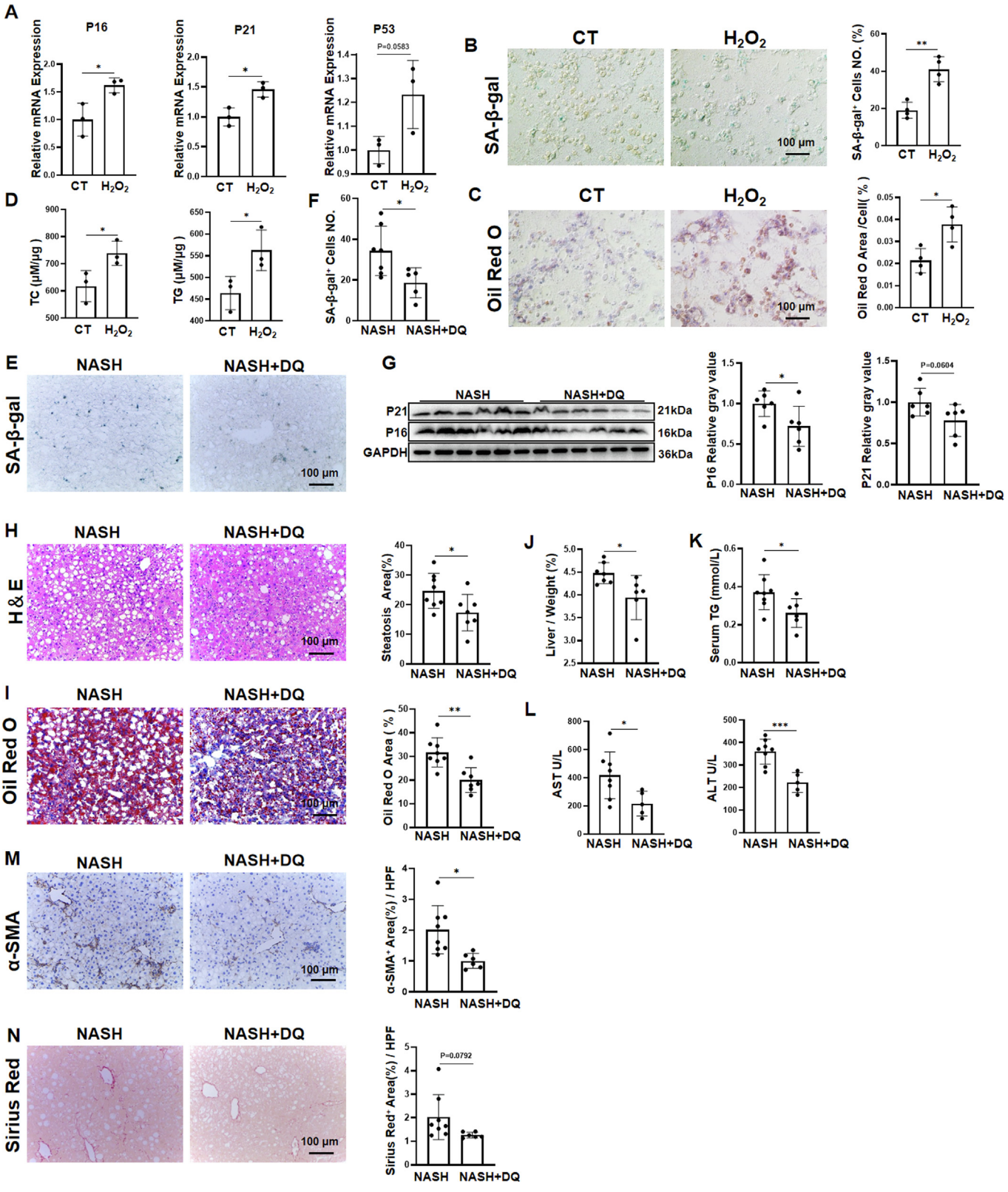
A
P16
P21
P53
P=0.0583
Relative mRNA Expression
CT
H2O2
B
SA-β-gal
CT
H2O2
100 μm
SA-β-gal+ Cells NO. (%)
C
Oil Red O
Oil Red O Area /Cell( % )
D
TC (μM/μg )
TG (μM/μg )
F
SA-β-gal+ Cells NO.
NASH
NASH+DQ
E
SA-β-gal
G
P21
P16
GAPDH
21kDa
16kDa
36kDa
P16 Relative gray value
P21 Relative gray value
P=0.0604
H
H&E
Steatosis Area(%)
J
Liver / Weight (%)
K
Serum TG (mmol/L)
I
Oil Red O
Oil Red O Area ( % )
L
AST U/L
ALT U/L
M
α-SMA
α-SMA+ Area(%) / HPF
N
Sirius Red
Sirius Red+ Area(%) / HPF
P=0.0792

mice. The findings revealed that, in comparison to the control group, NASH mice displayed heightened HES1 expression and significant co-localization with $LY6G^+$ neutrophils (Fig. 5A, B). To corroborate this observation, we harvested neutrophils from the bone marrow of NASH mice and analyzed the expression of Notch markers HES1 and HEY1. We ascertained that their expression was elevated in neutrophils from NASH mice (Fig. 5C), signifying that Notch signaling in neutrophils is amplified during NASH. Furthermore, we examined the impact of inhibiting Notch signaling in neutrophils on the formation of NETs both in vivo and in vitro. First, we isolated neutrophils from peripheral blood of healthy subjects and treated them with DAPT for 24 h in vitro to inhibit Notch. The efficiency of inhibition was confirmed by assessing HES1 and HEY1 expression levels, demonstrating that both 5 μM and 15 μM of DAPT decreased the expression of the Notch signaling pathway (Fig. 5D). Consequently, we selected 5 μM for further experiments. Then, neutrophils were stimulated with PMA for 2 h after Notch knockdown (Fig. 5E) to observe the effect of Notch knockdown on NETs formation. Through the measurement of NETs-dsDNA concentration in the culture medium, we determined that the inhibition of Notch signaling suppressed the formation of NETs (Fig. 5F). *Lyz2-Cre; RBP-J*$^{flox/flox}$ (RBPJ-KO) mice effectively eliminate Notch expression in neutrophils in vivo, thus we employed this genotype for our in vivo studies. Post isolation of bone marrow neutrophils and stimulation with PMA for 2 h or overnight culture without stimulation, we measured the concentration of NETs-dsDNA in the culture medium, obtaining results congruent with the in vitro experiment (Fig. 5G). PAD4 has been demonstrated to catalyse the citrullination of histones, thereby facilitating the formation of NETs, and it is considered to be a pivotal protein in this process. We hypothesised that Notch may modulate the formation of NETs by regulating PAD4 expression. To investigate this, we assessed the RNA and protein levels of PAD4 in bone marrow neutrophils from RBPJ-KO mice, revealing a significant reduction in PAD4 expression compared to wild-type mice (Fig. 5H-J). Consequently, our findings indicate that Notch signaling inhibits NET formation through the regulation of PAD4. Based on this, we established a NASH model using RBPJ-KO mice and detected the expression levels of NETs markers MPO and Cith3 in liver tissue by Western blot (Fig. 5K, L). We found that their expression in the livers of RBPJ-KO mice was inhibited. Simultaneously, we conducted transcriptome sequencing on the liver samples of RBPJ-KO mice. Both KEGG enrichment analysis and GSEA showed that NETs formation-related pathways were inhibited (Fig. 5M, N), while GSEA suggested that pathways related to leukocyte activation, proliferation, differentiation, and intercellular adhesion were activated (Fig. 5O). These findings suggest that inhibiting Notch signaling diminishes NETs generation associated with NASH.

*Disruption of Notch signaling reduces cellular senescence*

Based on the aforementioned findings, we determined that NETs influence liver senescence and steatosis in NASH, with a noticeable reduction in NETs formation in RBPJ-KO NASH mice. Therefore, we delved deeper into the alterations in liver senescence and steatosis in this model. First, by analyzing the transcriptome sequencing results of liver tissue, upon analyzing liver tissue transcriptome sequencing results, we identified that SASP-related pathways, DNA damage-induced senescence, oxidative stress-induced senescence, and cell senescence-related pathways were suppressed in the RBPJ-KO group (Fig. 6A). Subsequently, we assessed the expression levels of representative SASP molecules at both protein and mRNA levels utilizing Western blot (Fig. 6B, C) and qPCR (Fig. 6D), respectively, and discovered that liver senescence was mitigated in RBPJ-KO NASH mice. In addition, we executed SA-β-gal staining on liver tissue sections, revealing that liver senescence in RBPJ-KO NASH mice was diminished in comparison to control NASH mice (Fig. 6E). These findings imply that the activation of Notch signaling during NASH may foster the formation of NETs, consequently inducing liver senescence.

*Notch blocking alleviates liver inflammation and lipid deposition*

The accumulation of liver lipids and inflammatory infiltration constitute key pathological features of NASH. Thus, our research primarily focuses on whether blocking neutrophil-derived Notch could mitigate the progression of liver Steatosis in NASH mice. The Nile red staining of liver sections indicated a reduction in lipid deposition in the RBPJ-KO group compared to the control group (Fig. 7A, B). Correspondingly, the SAF score implied a decreased severity of inflammation and fibrosis in RBPJ-KO mice (Fig. 7C). Transcriptome sequencing analysis of livers from RBPJ-KO and wild-type NASH mice revealed that the top 20 significant signaling pathways enriched by GO predominantly pertained to lipid metabolism (Fig. 7D). It also suggested that blocking neutrophil-derived Notch signaling could augment the oxidation, decomposition, metabolism, and beta-oxidation of liver fatty acids (Fig. 7E), thus reducing liver lipid deposition. At the same time, inflammatory type I interferon receptor binding related pathways were inhibited in the liver tissues of the RBPJ-KO group, and nuclear receptor signaling was down-regulated in the same group (Fig. 7F). Immunofluorescence staining showed that the number of infiltrated neutrophils in the liver was significantly reduced (Fig. 7G, H). These suggest that RBPJ-KO NASH mice have reduced hepatic inflammatory infiltration and lipid deposition.

**Fig. 4.** Clearance of senescent cells decelerated senescence-induced hepatic steatosis. (A) Relative mRNA expression levels of P16, P21 and P53 ($P$ = 0.0583) in primary hepatocytes after solvent control and $H_2O_2$ treatment were determined using qPCR; β-actin served as an internal control ($n$ = 3). (B) SA-β-gal staining of primary hepatocytes after solvent control and $H_2O_2$ treatment and positive cells were quantitatively compared ($n$ = 4). Scale bar: 100 μm. (C) Oil Red O staining of in primary hepatocytes after solvent control and $H_2O_2$ treatment and positive area were quantitatively compared ($n$ = 4). Scale bar: 100 μm. (D) Hepatic TC and TG levels of primary hepatocytes after solvent control and $H_2O_2$ treatment ($n$ = 3). (E) SA-β-gal staining of NASH mice liver tissue after treated with solvent control and DQ gastric irrigation, and (F) positive cells were quantitatively compared ($n$ = 4). Scale bar: 100 μm. (G) Western blot analysis of P21 ($P$ = 0.0604) and P16 protein expression in liver tissue of NASH mice with solvent control or DQ gastric irrigation, and (I) the gray ratio of P21, P16 and GAPDH was quantitatively compared ($n$ = 6). (H) H&E staining of liver tissue of NASH mice with solvent control or DQ gastric irrigation, and steatosis area were quantitatively compared ($n$ = 7 to 8). Scale bar: 100 μm. (I) Oil Red O staining of liver tissue of NASH mice with solvent control or DQ gastric irrigation, and positive area were quantitatively compared ($n$ = 7 to 8). Scale bar: 100 μm. (J) Liver to body weight ratio of NASH mice with solvent control or DQ gastric irrigation ($n$ = 6). (K) Serum AST and ALT levels of NASH mice with solvent control or DQ gastric irrigation ($n$ = 6 to 8). (L) Serum TG level of NASH mice with solvent control or DQ gastric irrigation ($n$ = 5 to 8). (M) α-SMA staining of liver tissue of NASH mice with solvent control or DQ gastric irrigation, and positive area were quantitatively compared ($n$ = 6 to 8). Scale bar: 100 μm. (N) Sirius Red staining of liver tissue of NASH mice with solvent control or DQ gastric irrigation, and positive area were quantitatively compared ($P$ = 0.0792, $n$ = 6 to 8). Scale bar: 100 μm. Bars represent means ± SD; $^*P < 0.05$, $^{**}P < 0.01$, $^{***}P < 0.001$, ns, not significant.

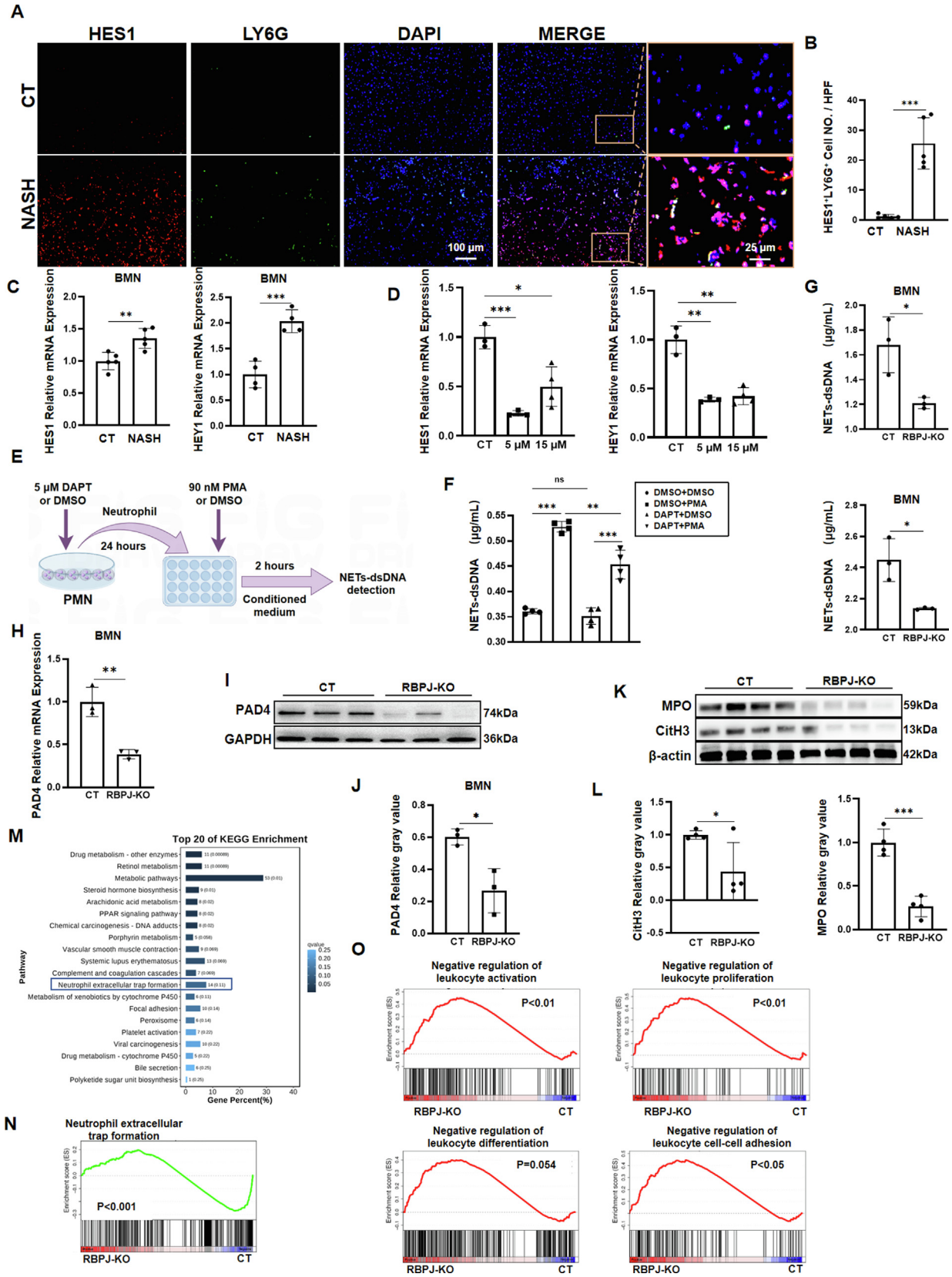
A
HES1
LY6G
DAPI
MERGE
CT
NASH
100 μm
25 μm
B
HES1+LY6G+ Cell NO. / HPF
CT NASH
C
BMN
HES1 Relative mRNA Expression
HEY1 Relative mRNA Expression
CT NASH
D
HES1 Relative mRNA Expression
HEY1 Relative mRNA Expression
CT 5 μM 15 μM
G
BMN
NETs-dsDNA (μg/mL)
CT RBPJ-KO
E
5 μM DAPT or DMSO
90 nM PMA or DMSO
Neutrophil
24 hours
2 hours
PMN
Conditioned medium
NETs-dsDNA detection
F
NETs-dsDNA (μg/mL)
DMSO+DMSO
DMSO+PMA
DAPT+DMSO
DAPT+PMA
H
BMN
PAD4 Relative mRNA Expression
CT RBPJ-KO
I
CT RBPJ-KO
PAD4
GAPDH
74kDa
36kDa
K
CT RBPJ-KO
MPO
CitH3
β-actin
59kDa
13kDa
42kDa
J
BMN
PAD4 Relative gray value
CT RBPJ-KO
L
CitH3 Relative gray value
MPO Relative gray value
CT RBPJ-KO
M
Top 20 of KEGG Enrichment
Drug metabolism - other enzymes
Retinol metabolism
Metabolic pathways
Steroid hormone biosynthesis
Arachidonic acid metabolism
PPAR signaling pathway
Chemical carcinogenesis - DNA adducts
Porphyrin metabolism
Vascular smooth muscle contraction
Systemic lupus erythematosus
Complement and coagulation cascades
Neutrophil extracellular trap formation
Metabolism of xenobiotics by cytochrome P450
Focal adhesion
Peroxisome
Platelet activation
Viral carcinogenesis
Drug metabolism - cytochrome P450
Bile secretion
Polyketide sugar unit biosynthesis
Pathway
Gene Percent(%)
qvalue
O
Negative regulation of leukocyte activation
P<0.01
Negative regulation of leukocyte proliferation
P<0.01
Negative regulation of leukocyte differentiation
P=0.054
Negative regulation of leukocyte cell-cell adhesion
P<0.05
RBPJ-KO CT
N
Neutrophil extracellular trap formation
P<0.001
RBPJ-KO CT

## Discussion

Given the surging systemic metabolic risk factors and continuous rise in prevalence rates, NAFLD poses a significant public health burden globally. NASH, a severe form of NAFLD, is distinguished by pronounced steatosis, inflammation, and fibrosis. Regrettably, once patients progress to the NASH stage, their condition is often irreversible and may even advance to cirrhosis or liver cancer. However, current clinical interventions primarily target symptomatic relief, such as mitigating liver damage and managing metabolic disorders, strategies that seldom result in comprehensive improvement. Owing to the multifaceted etiology of NASH, disease progression may be influenced by numerous factors and targets, rendering single-drug therapies inadequate for most patients. Consequently, a holistic comprehension of the cellular underpinnings and molecular contrivances of NASH onset is paramount in offering robust scientific proof for comprehensive and effective treatments.

Inflammatory hepatic steatosis alongside progressive liver fibrosis are the most prominent pathological features of NASH. The activation of various inflammatory cells, including neutrophils, drives the release of pro-inflammatory cytokines and oxidative stress, which leads to hepatic inflammation and dysregulation of lipid metabolism [31]. The creation of NETs by neutrophils is a crucial pathway for preserving an inflammatory state, exerting its effects post-damage [32–34]. Excessive NETs constitute harmful factors, intensifying liver damage and promoting cancer progression [35–38]. Initial investigations into NETs' role in fatty liver disease were conducted by Allan Tsung and his colleagues [11]. Their research indicated a significant neutrophil influx into the liver during the early stages of NAFLD, with NETs produced by inflammatory stimuli accelerating progression to NASH-associated liver cancer. Further studies demonstrated that NETs contribute to this process, promoting the differentiation of immature $CD4^+$ T cells into regulatory T cells. Furthermore, research conducted by Liying Li and colleagues using a Methionine Choline Deficiency High-Fat diet (MCDHF) mouse model illustrated that inhibiting NET formation effectively mitigates liver inflammation and fibrosis [39]. In agreement with these findings, we confirmed a significant increase in NET-associated molecules such as free dsDNA, CitH3, and MPO in both NASH patients and mouse models.

Owing to the widespread prevalence and global impact of NAFLD, alongside population aging, the exploration of the connection between NASH and aging has garnered considerable interest. The aging process results in systemic metabolic disorders, including lipid metabolism imbalance and insulin resistance, which perpetually induce liver steatosis. In our prior research, we observed a significant exacerbation of lipid deposition in senescent livers [40]. Despite the rising number of studies investigating the correlation between NETs and NASH in recent years, none have concentrated on the association between NETs and senescent cells during NASH progression. In this study, we addressed this issue and discovered, for the first time, that NETs can expedite liver cell senescence. Utilizing drugs to eradicate senescent cells, we observed significant improvements in lipid metabolism and liver injury in diet-induced NASH livers in mice. Importantly, we were also able to elucidate, for the first time, the relationship between NETs-mediated hepatocyte senescence and lipotoxicity. We induced isolated cellular senescence in primary hepatocytes in vitro using $H_2O_2$, thereby excluding the influence of other factors from the liver microenvironment, and observed alterations in hepatocyte lipid metabolism. This may be related to $H_2O_2$-induced mitochondrial dysfunction, which impairs the activity of antioxidant enzymes, leading to lipid peroxidation and lipid accumulation in hepatocytes [41,42]. We observed an increase in the positive area of Oil Red O staining in senescent hepatocytes, accompanied by a rise in the intracellular levels of TC and TG, suggesting a significant escalation in lipid deposition within these cells. Additionally, we employed a wild-type mouse model of NASH, administering DQ via oral gavage to eliminate senescent cells, and observed a significant reduction in liver lipid deposition and fibrosis, with partial restoration of liver function. Based on these results, we deduced that senescent cells, induced by NETs during NASH progression, enhance liver lipotoxicity and intensify the advancement of NASH.

The Notch signaling pathway is a classical signaling cascade essential in maintaining liver homeostasis and modulating liver disease progression. Pajvani and colleagues demonstrated significant activation of hepatocyte Notch signaling in both patients with NASH and in a diet-induced NASH mouse model [43,44]. Our prior research has identified that Notch signaling, derived from non-parenchymal cells, notably LSECs, is substantially activated in NASH, and blocking Notch signaling in various cellular types can significantly curtail NASH progression [45–47]. Nonetheless, it remains to be clarified whether immune cells, such as neutrophils, also fall under the regulation of the Notch pathway. Interestingly, in this study, we discovered significant activation of neutrophil-derived Notch signaling in mice with NASH. Based on these observations, we employed a bone marrow-specific RBP-J knockout mouse model (*Lyz2-Cre; RBP-J*$^{flox/flox}$) for our NASH investigations. We observed significant reductions in liver inflammation, cellular senescence, and steatosis in these mice. Transcriptome sequencing of liver tissue indicated suppression of both NETs and cell senescence-related pathways in RBP-J KO mice, alongside activation of fatty acid oxidation, catabolism, metabolism, and β-oxidation pathways. Currently, there is no neutrophil-specific CRE mouse, we utilized *Lyz2-Cre* mice, which serve as myeloid cell marker mice similar to *Ela2-cre*, *Mrp8-Cre*, and *CD11c-Cre* used in previous studies, which introduces notable limitations to our

**Fig. 5.** Blocking Notch signaling diminished NASH-associated NETs. IF staining of HES1 (red), LY6G (green) and 4,6-diamidino-2-phenylindole (DAPI) (blue) in liver tissue of control and NASH mice, and (B) the positive fluorescent staining ratio of $HES1^+LY6G^+$ cells was quantified ($n$ = 5). (C) Relative mRNA expression levels of HES1 and HEY1 in bone marrow neutrophils of control and NASH mice were determined using qPCR; β-actin served as an internal control ($n$ = 5). (D) Relative mRNA expression levels of HES1 and HEY1 in neutrophils isolation from healthy subjects were determined using qPCR, which treated with solvent control or different concentration of DAPT (5 μM or15 μM) for 24 h in vitro; β-actin served as an internal control ($n$ = 3). (E) Schematic diagram of in vitro experimental steps examining the effect of blocking Notch signaling in neutrophils on NETs formation. (F) Concentration of NETs-dsDNA in the medium of neutrophils treated with solvent control(DMSO) and DAPT, which after 2 h stimulation of DMSO or PMA ($n$ = 4). (G) Concentration of NETs-dsDNA in the medium of neutrophils from control and RBPJ-KO mice stimulated with PMA for 2 h (up) and overnight without stimulation (down) ($n$ = 3). (H) Relative mRNA expression levels of PAD4 in BMN of control and NASH mice were determined using qPCR; β-actin served as an internal control ($n$ = 3). (I) Western blot analysis of PAD4 in BMN of control and RBPJ-KO mice, and (J) the gray ratio of PAD4 and GAPDH was quantitatively compared ($n$ = 4). (K) Western blot analysis of MPO and CitH3 in liver tissue of control and RBPJ-KO mice, and (L) the gray ratio of MPO, CitH3 and GAPDH was quantitatively compared ($n$ = 4). (M) Top 20 of KEGG enrichment analysis of transcriptome sequencing in liver tissue of control and RBPJ-KO mice with NASH model. (N) GSEA of neutrophil extracellular trap formation-related pathways in control and RBPJ-KO mice with NASH model. (O) GSEA of leukocyte activation, proliferation, differentiation, and cell–cell adhesion-related pathways in control and RBPJ-KO mice with NASH model. Bars represent means ± SD; $^*P < 0.05$, $^{**}P < 0.01$, $^{***}P < 0.001$, ns, not significant.

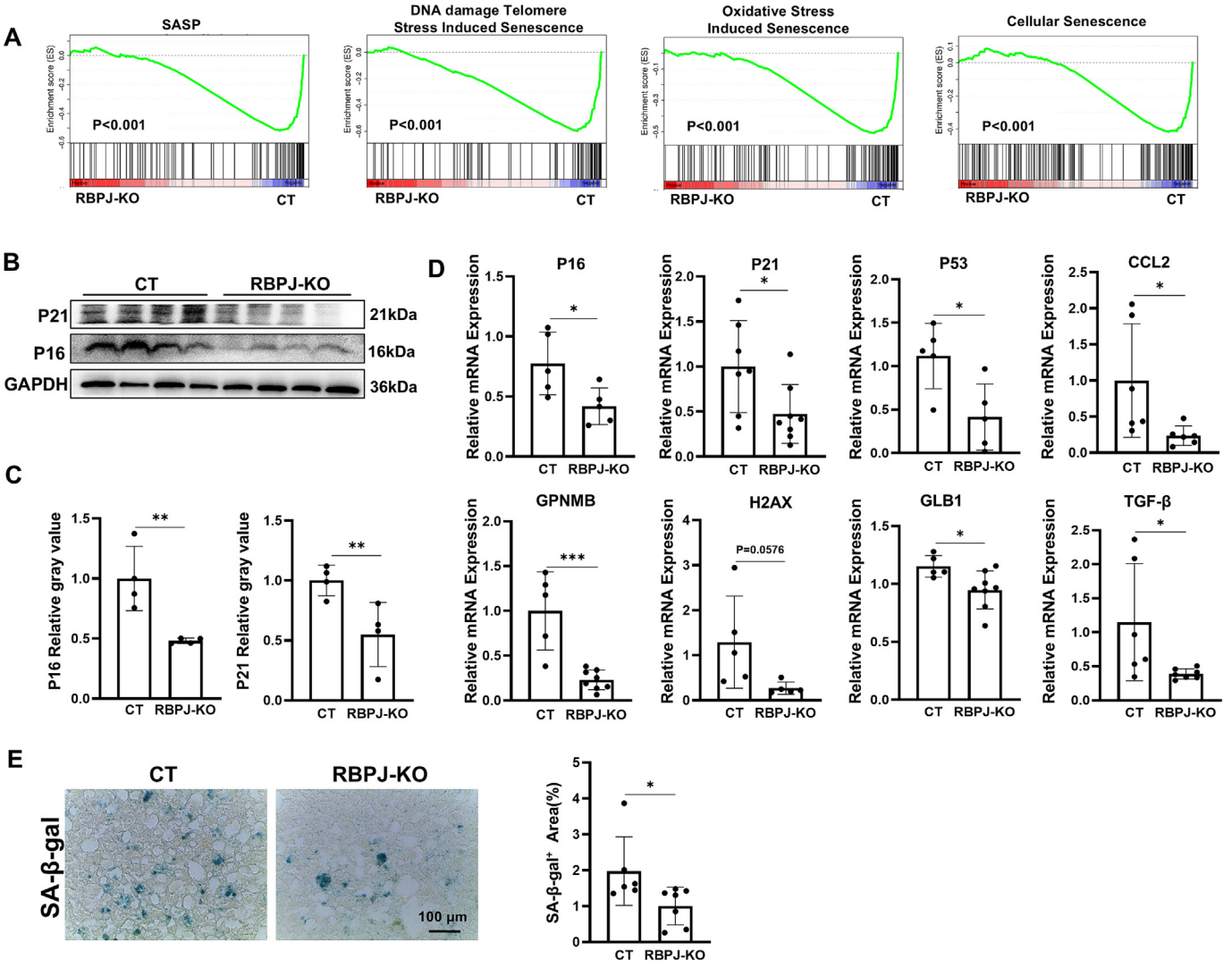


**Fig. 6.** Disruption of Notch signaling reduced cellular senescence. (A) GSEA of hepatocyte senescence, SASP, DNA damage-induced senescence, and oxidative stress-induced senescence in the liver of control and RBPJ-KO mice models of NASH. (B) Western blot analysis of P16 and P21 in liver tissue of control and RBPJ-KO mice, and (C) the gray ratio of P16, P21 and GAPDH was quantitatively compared ($n$ = 4). (D) Relative mRNA expression levels of P16, P21, P53, CCL2, GPNMB, H2AX (P = 0.0576), GLB1 and TGF-β in liver tissue of control and NASH mice were determined using qPCR; β-actin served as an internal control ($n$ = 5). (E) SA-β-gal staining of liver tissue of control and RBPJ-KO mice models of NASH, and positive cells were quantitatively compared ($n$ = 6 to 7). Scale bar: 100 μm. Bars represent means ± SD; $^{*}P < 0.05$, $^{**}P < 0.01$, $^{***}P < 0.001$.

research. Ou and his colleagues depleted neutrophils using a mouse model with anti-Ly-6G antibodies, finding that neutrophil depletion significantly reduced liver lipid accumulation and inflammation in diet-induced NASH [48]. Though we did not use the same animal model, our results showing NETs-induced lipid deposition are consistent with their conclusion. Recent study shows that macrophages in *Lyz2-Cre; RBP-J*$^{flox/flox}$ mice contribute to the progression of NAFLD [47]. Therefore, our study cannot exclude the potential impact Notch signaling alterations in other myeloid cells and can only concentrate on the changes occurring within neutrophils. Nevertheless, our study targeting notch signaling in neutrophils is still very meaningful.

## Conclusion

We discovered that neutrophil-derived Notch signaling can foster NETs formation, thus exacerbating cellular senescence and lipotoxicity during NASH. As the deployment of Notch inhibitors is gradually being incorporated into clinical practice, our research outcomes will furnish novel strategies and targets for the intervention of NAFLD/NASH.

## Declaration of competing interest

The authors declare that they have no known competing financial interests or personal relationships that could have appeared to influence the work reported in this paper.

## Acknowledgments

This work was supported by grants from National Natural Science Foundation of China (82325007, 92468202, 82370620, 82400666, 82300703, 82400670) and the National Key Research and Development Program of China (2021YFA1100502). We would thank Prof. Han Hua for *Lyz2-Cre*; *RBPJ*$^{flox}$ mice.

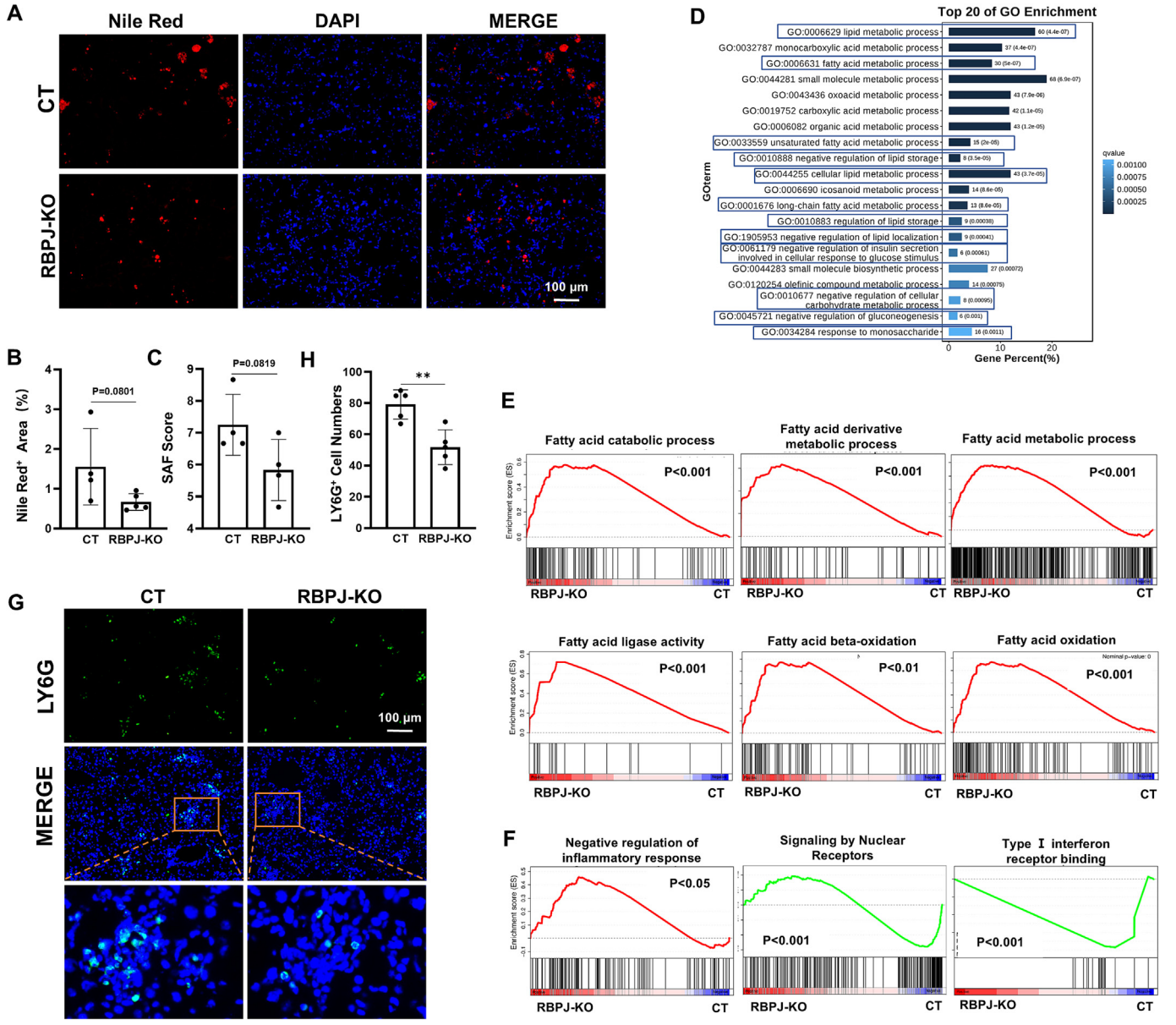


**Fig. 7.** Notch blocking alleviates liver inflammation and lipid deposition. (A) IF staining of Nile red (red) and 4,6-diamidino-2-phenylindole (DAPI) (blue) in liver tissue of control and RBPJ-KO mice models of NASH, and (B) the positive fluorescent staining ratio of Nile red$^+$ area was quantified ($P = 0.0801$; $n = 4$ to 5). (C) SAF score of liver tissue in NASH models of control and RBPJ-KO mice ($P = 0.0819$; $n = 4$). (D) GO enrichment analysis of transcriptome sequencing of liver tissue in NASH models of control and RBPJ-KO mice. (E) GSEA of fatty acid oxidation, decomposition, metabolism, and β-oxidation processes in the liver of NASH models of control and RBPJ-KO mice. (F) GSEA of inflammatory-related pathways in NASH models of control and RBPJ-KO mice. (G) IF staining of LY6G (green) and DAPI (blue) in liver tissue of control and RBPJ-KO mice models of NASH, and (H) the positive fluorescent staining ratio of LY6G$^+$ cells was quantified ($n = 4$ to 5). Bars represent means ± SD; $^*P < 0.05$, $^{**}P < 0.01$, $^{***}P < 0.001$.

## Appendix A. Supplementary data

Supplementary data to this article can be found online at https://doi.org/10.1016/j.jare.2025.03.015.

## References

[1] Wong VW, Ekstedt M, Wong GL, Hagström H. Changing epidemiology, global trends and implications for outcomes of NAFLD. J Hepatol 2023;79(3):842–52.
[2] Devarbhavi H, Asrani SK, Arab JP, Nartey YA, Pose E, Kamath PS. Global burden of liver disease: 2023 update. J Hepatol 2023;79(2):516–37.
[3] Younossi ZM, Golabi P, Paik JM, Henry A, Van Dongen C, Henry L. The global epidemiology of nonalcoholic fatty liver disease (NAFLD) and nonalcoholic steatohepatitis (NASH): a systematic review. Hepatology (Baltimore, MD) 2023;77(4):1335–47.
[4] Wong VW, Ekstedt M, Wong GL, Hagstrom H. Changing epidemiology, global trends and implications for outcomes of NAFLD. J Hepatol 2023;79(3):842–52.
[5] Llovet JM, Willoughby CE, Singal AG, Greten TF, Heikenwalder M, El-Serag HB, et al. Nonalcoholic steatohepatitis-related hepatocellular carcinoma: pathogenesis and treatment. Nat Rev Gastroenterol Hepatol 2023;20(8):487–503.
[6] Peiseler M, Schwabe R, Hampe J, Kubes P, Heikenwalder M, Tacke F. Immune mechanisms linking metabolic injury to inflammation and fibrosis in fatty liver disease - novel insights into cellular communication circuits. J Hepatol 2022;77(4):1136–60.
[7] Harrison SA, Allen AM, Dubourg J, Noureddin M, Alkhouri N. Challenges and opportunities in NASH drug development. Nat Med 2023;29(3):562–73.
[8] Hwang S, Yun H, Moon S, Cho YE, Gao B. Role of Neutrophils in the Pathogenesis of Nonalcoholic Steatohepatitis. Front Endocrinol (Lausanne) 2021;12:751802.
[9] Loomba R, Friedman SL, Shulman GI. Mechanisms and disease consequences of nonalcoholic fatty liver disease. Cell 2021;184(10):2537–64.

[10] Powell EE, Wong VW, Rinella M. Non-alcoholic fatty liver disease. Lancet 2021;397(10290):2212–24.
[11] van der Windt DJ, Sud V, Zhang H, Varley PR, Goswami J, Yazdani HO, et al. Neutrophil extracellular traps promote inflammation and development of hepatocellular carcinoma in nonalcoholic steatohepatitis. Hepatology 2018;68(4):1347–60.
[12] Borregaard N. Neutrophils, from marrow to microbes. Immunity 2010;33(5):657–70.
[13] Cho Y, Bukong TN, Tornai D, Babuta M, Vlachos IS, Kanata E, et al. Neutrophil extracellular traps contribute to liver damage and increase defective low-density neutrophils in alcohol-associated hepatitis. J Hepatol 2023;78(1):28–44.
[14] Huang H, Tohme S, Al-Khafaji AB, Tai S, Loughran P, Chen L, et al. Damage-associated molecular pattern-activated neutrophil extracellular trap exacerbates sterile inflammatory liver injury. Hepatology 2015;62(2):600–14.
[15] Li X, Gao Q, Wu W, Hai S, Hu J, You J, et al. FGL2-MCOLN3-Autophagy Axis-Triggered Neutrophil Extracellular Traps Exacerbate Liver Injury in Fulminant Viral Hepatitis. Cell Mol Gastroenterol Hepatol 2022;14(5):1077–101.
[16] Ye D, Yao J, Du W, Chen C, Yang Y, Yan K, et al. Neutrophil Extracellular Traps Mediate Acute Liver Failure in Regulation of miR-223/Neutrophil Elastase Signaling in Mice. Cell Mol Gastroenterol Hepatol 2022;14(3):587–607.
[17] Zhu W, Fan C, Dong S, Li X, Chen H, Zhou W. Neutrophil extracellular traps regulating tumorimmunity in hepatocellular carcinoma. Front Immunol 2023;14:1253964.
[18] Campisi J, D'Adda DFF. Cellular senescence: when bad things happen to good cells. Nat Rev Mol Cell Biol 2007;8(9):729–40.
[19] Huang W, Hickson LJ, Eirin A, Kirkland JL, Lerman LO. Cellular senescence: the good, the bad and the unknown. Nat Rev Nephrol 2022;18(10):611–27.
[20] Salama R, Sadaie M, Hoare M, Narita M. Cellular senescence and its effector programs. Genes Dev 2014;28(2):99–114.
[21] Cohn RL, Gasek NS, Kuchel GA, Xu M. The heterogeneity of cellular senescence: insights at the single-cell level. Trends Cell Biol 2023;33(1):9–17.
[22] Hernandez-Segura A, Nehme J, Demaria M. Hallmarks of Cellular Senescence. Trends Cell Biol 2018;28(6):436–53.
[23] Zeng Q, Gong Y, Zhu N, Shi Y, Zhang C, Qin L. Lipids and lipid metabolism in cellular senescence: Emerging targets for age-related diseases. Ageing Res Rev 2024;97:102294.
[24] Baboota RK, Rawshani A, Bonnet L, Li X, Yang H, Mardinoglu A, et al. BMP4 and Gremlin 1 regulate hepatic cell senescence during clinical progression of NAFLD/NASH. Nat Metab 2022;4(8):1007–21.
[25] Nakano Y, Johmura Y. Targeting cellular senescence as a therapeutic approach in non-alcoholic steatohepatitis. Ann Hepatol 2023;28(2):100900.
[26] Adams JM, Jafar-Nejad H. The Roles of Notch Signaling in Liver Development and Disease. Biomolecules 2019;9(10).
[27] Geisler F, Strazzabosco M. Emerging roles of Notch signaling in liver disease. Hepatology 2015;61(1):382–92.
[28] Romeo S. Notch and Nonalcoholic Fatty Liver and Fibrosis. N Engl J Med 2019;380(7):681–3.
[29] Fang ZQ, Ruan B, Liu JJ, Duan JL, Yue ZS, Song P, et al. Notch-triggered maladaptation of liver sinusoidal endothelium aggravates nonalcoholic steatohepatitis through endothelial nitric oxide synthase. Hepatology 2022.
[30] Duan JL, Ruan B, Yan XC, Liang L, Song P, Yang ZY, et al. Endothelial Notch activation reshapes the angiocrine of sinusoidal endothelia to aggravate liver fibrosis and blunt regeneration in mice. Hepatology 2018;68(2):677–90.
[31] Zhao R, Zhang J, Ma J, Qu Y, Yang Z, Yin Z, et al. cGAS-activated endothelial cell-T cell cross-talk initiates tertiary lymphoid structure formation. Sci Immunol 2024;9(98):k2612.
[32] Castanheira F, Kubes P. Neutrophils and NETs in modulating acute and chronic inflammation. Blood 2019;133(20):2178–85.
[33] Papayannopoulos V. Neutrophil extracellular traps in immunity and disease. Nat Rev Immunol 2018;18(2):134–47.
[34] Wang H, Kim SJ, Lei Y, Wang S, Wang H, Huang H, et al. Neutrophil extracellular traps in homeostasis and disease. Signal Transduct Target Ther 2024;9(1):235.
[35] Wang Z, Chen C, Shi C, Zhao X, Gao L, Guo F, et al. Cell membrane derived liposomes loaded with DNase I target neutrophil extracellular traps which inhibits colorectal cancer liver metastases. J Control Release 2023;357:620–9.
[36] Liu Y, Pu X, Qin X, Gong J, Huang Z, Luo Y, et al. Neutrophil Extracellular Traps Regulate HMGB1 Translocation and Kupffer Cell M1 Polarization During Acute Liver Transplantation Rejection. Front Immunol 2022;13:823511.
[37] Yang LY, Luo Q, Lu L, Zhu WW, Sun HT, Wei R, et al. Increased neutrophil extracellular traps promote metastasis potential of hepatocellular carcinoma via provoking tumorous inflammatory response. J Hematol Oncol 2020;13(1):3.
[38] Nolan E, Malanchi I. Neutrophil 'safety net' causes cancer cells to metastasize and proliferate. Nature 2020;583(7814):32–3.
[39] Zhao X, Yang L, Chang N, Hou L, Zhou X, Yang L, et al. Neutrophils undergo switch of apoptosis to NETosis during murine fatty liver injury via S1P receptor 2 signaling. Cell Death Dis 2020;11(5):379.
[40] Duan JL, Liu JJ, Ruan B, Ding J, Fang ZQ, Xu H, et al. Age-related liver endothelial zonation triggers steatohepatitis by inactivating pericentral endothelium-derived C-kit. Nat Aging 2023;3(3):258–74.
[41] Myint M, Oppedisano F, De Giorgi V, Kim BM, Marincola FM, Alter HJ, et al. Inflammatory signaling in NASH driven by hepatocyte mitochondrial dysfunctions. J Transl Med 2023;21(1):757.
[42] Retter A, Singer M, Annane D. "The NET effect": Neutrophil extracellular traps-a potential key component of the dysregulated host immune response in sepsis. Crit Care 2025;29(1):59.
[43] Zhu C, Kim K, Wang X, Bartolome A, Salomao M, Dongiovanni P, et al. Hepatocyte Notch activation induces liver fibrosis in nonalcoholic steatohepatitis. Sci Transl Med 2018;10(468).
[44] Yu J, Zhu C, Wang X, Kim K, Bartolome A, Dongiovanni P, et al. Hepatocyte TLR4 triggers inter-hepatocyte Jagged1/Notch signaling to determine NASH-induced fibrosis. Sci Transl Med 2021;13(599).
[45] Fang ZQ, Ruan B, Liu JJ, Duan JL, Yue ZS, Song P, et al. Notch-triggered maladaptation of liver sinusoidal endothelium aggravates nonalcoholic steatohepatitis through endothelial nitric oxide synthase. Hepatology 2022;76(3):742–58.
[46] Yue Z, Jiang Z, Ruan B, Duan J, Song P, Liu J, et al. Disruption of myofibroblastic Notch signaling attenuates liver fibrosis by modulating fibrosis progression and regression. Int J Biol Sci 2021;17(9):2135–46.
[47] Ding J, Xu M, Du W, Fang ZQ, Xu H, Liu JJ, et al. Myeloid-specific blockade of Notch signaling ameliorates nonalcoholic fatty liver disease in mice. Int J Biol Sci 2023;19(6):1941–54.
[48] Ou R, Liu J, Lv M, Wang J, Wang J, Zhu L, et al. Neutrophil depletion improves diet-induced non-alcoholic fatty liver disease in mice. Endocrine 2017;57(1):72–82.